PERFORMANCE OF CODED APERTURE X-RAY OPTICS WITH LOW EMITTANCE BEAM AT CESRTA*

J.W. Flanagan†, H. Fukuma, S. Hiramatsu, H. Ikeda, K. Kanazawa, T. Mitsuhashi, J. Urakawa
KEK, Tsukuba, Ibaraki 305-0801, Japan
G.S. Varner, U. Hawaii, Honolulu, HI 96822, USA
J.P. Alexander, W.H. Hopkins, B. Kreis, M.A. Palmer, D.P. Peterson,
CLASSE, Cornell U., Ithaca, NY 14853, USA

Abstract

We are working on the development of a high-speed x-ray beam profile monitor for high-resolution and fast response for beam profile measurements to be used at CesrTA and SuperKEKB.[1] The optics for the monitor are based on coded-aperture imaging, which should permit broad-spectrum, low-distortion measurements to maximize the observable photon flux per bunch. Coupled with a high-speed digitizer system, the goal is to make turn-by-turn, bunch-by-bunch beam profile measurements. Following initial tests with a low-resolution mask at large beam sizes (vertical size $\approx 200\,\mu$m), a high-resolution mask has been made for use with low-emittance beams (vertical size $\approx 10\,\mu$m) at CesrTA. We discuss the methods for analyzing the coded aperture mask data, and some preliminary performance results of the use of the high-resolution mask on the low-emittance CesrTA beam in January 2009.

INTRODUCTION

Our goal is to develop an x-ray monitor for transverse bunch-by-bunch beam profile monitoring, with high resolution (a few μm) and fast response, suitable for bunch-by-bunch diagnostics at present and future lepton accelerators, such as CesrTA, SuperKEKB, or the ILC damping ring. To meet these requirements, we are developing an x-ray imaging system based on coded aperture imaging.

Coded aperture imaging is a technique well-developed among x-ray astronomers[2], which provides the spatial resolution of a pinhole camera, but with much greater x-ray photon collection efficiency. It consists of a pseudo-random array of pinholes, which project a mosaic of pinhole camera images onto a detector. This image is then decoded using the known mask pattern to reconstruct the original image. One example of such a pattern is the Uniformly Redundant Array (URA)[3], which features an open aperture of 50% with an even sampling of spatial frequencies in the non-diffractive limit. The coded aperture pattern used in the January 2009 tests at CesrTA is shown in Fig. 1; it is composed of $0.7\,\mu$m Au in the mask regions, on a $2.5\,\mu$m Si substrate. It was made by Applied Nanotools, Inc. The minimum vertical feature size is $10\,\mu$m, with a horizontal width of $1200\,\mu$m.
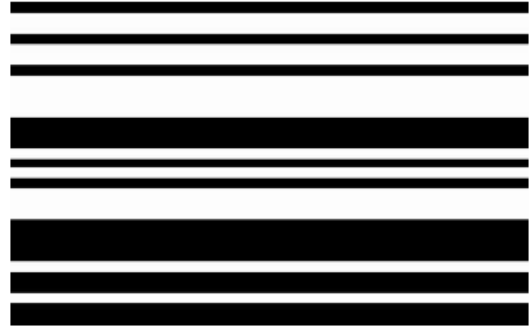
Figure 1: Coded aperture test mask used in January 2009 beam test at CesrTA. (Aspect ratio not to scale.)

BEAM LINE, DETECTOR, FLUX

The beam line used in the January, 2009 tests was the D Line, ordinarily used by CHESS light-source users. This beam line views the positron beam. The parameters of the beam line are shown in Table 1. The x-ray optics (coded aperture mask, Fresnel zone plate, movable slits) are mounted in a holder 4.29 m downstream of the beam. The holder can be moved to place the desired optical element in the beam line. The beam line is entirely evacuated from beam source point to detector. Other than the optical elements, the only other item in the beam line is a $4\,\mu$m diamond window located just upstream of the detector, to separate the vacuum on the detector side from the clean vacuum on the beam side.

Table 1: Source parameters at D Line of CesrTA.

Parameter	Value
Beam Energy	2.085 GeV
Bend Radius	31.65 m
Bunch Current	≈ 1 mA/bunch (variable)
Vertical Beam Size	$\approx 10\,\mu$m (target)
Beam-to-Mask Distance	4.29 m
Mask-to-Detector Distance	10.71 m

The detector is an InGaAs array produced by Fermionics, Inc., which features $25\,\mu$m $\times 500\,\mu$m pixels on a $50\,\mu$m pitch. The thickness of the InGaAs layer is $3.5\,\mu$m, which captures about 90% of the flux that reaches it after passing through the diamond window, and other layers on the chip above the InGaAs layer. The total detectable flux over a $25\,\mu$m $\times 500\,\mu$m area in the InGaAs layer is esti-

mated to be about 550 photons/turn/mA/bunch with no x-ray optical elements in the way; thus a wideband, large-open-aperture technique is necessary for bunch-by-bunch, turn-by-turn measurements. With the coded aperture in place, the average estimated flux per pixel is about 160 photons/turn/mA/bunch. (The calculated flux estimates for the coded aperture and the bare beam cases agree roughly with measurements of the statistical fluctuations in the detected signal.) The detectable spectrum lies largely between 1 and 5 keV.

For future bunch-by-bunch use at CesrTA, a high-speed readout is being developed[4], but for preliminary checking of the x-ray system[5] and beam sizes, a single Fermionics pixel was mechanically scanned across the imaging plane while being read out in DC mode with a picoammeter. These DC scan data are used here.

Simulation Method

Coded aperture imaging, as traditionally used in x-ray astronomy, operates far from the diffraction region. As has been noted previously[1], diffraction effects cannot be ignored for the x-ray wavelengths and mask feature sizes we are using. In this subsection, we describe the formalism used to simulate the detected image.

Following K.J. Kim's formulation[6], the σ and π components of the complex wavefront amplitude of the component of synchrotron radiation (SR) with angular frequency ω can be written as

$$\left[\begin{array}{c} A_\sigma \\ A_\pi \end{array} \right] = \frac{\sqrt{3}}{2\pi} \gamma \frac{\omega}{\omega_c} \left(1 + X^2 \right) (-i) \left[\begin{array}{c} K_{2/3}(\eta) \\ \frac{iX}{\sqrt{1+X^2}} K_{1/3}(\eta) \end{array} \right],$$

where

$$X = \gamma\psi,$$

$$\eta = \frac{1}{2} \frac{\omega}{\omega_c} \left(1 + X^2 \right)^{3/2},$$

and γ is the Lorentz factor for the particle beam. Also, ω_c is the critical angular frequency of the SR, ψ is the vertical angle off the plane of revolution of the beam, and K are the modified Bessel functions. The angular density of the spectral flux in frequency band $\frac{\Delta\omega}{\omega}$ is then

$$\left[\begin{array}{c} \frac{d^2 F_\sigma}{d\theta d\psi} \\ \frac{d^2 F_\pi}{d\theta d\psi} \end{array} \right] = \alpha \frac{\Delta\omega}{\omega} \frac{I}{e} \left| \begin{array}{c} A_\sigma \\ A_\pi \end{array} \right|^2,$$

where $d\theta$ represents the horizontal angle element, α is the fine-structure constant, I is the accelerator beam current, and e is the charge of the electron.

To calculate the flux measured at the detector, we propagate the wavefronts $A_{\sigma,\pi}$ through the model of the beamline, taking account of the attenuation and phase shifts due to the various materials and pathlengths along the way. For a one-dimensional mask, the path integral in the vertical direction from a point in the source distribution to a point on

the detector can be written using the Kirchhoff approximation as (see, *e.g.*, [7], Eq. 7.18 or [8], Eq. 9.132):

$$\begin{aligned} A_{\sigma,\pi}(y_d) \quad &= \frac{iA_{\sigma,\pi}(\text{source})}{\lambda} \int_{\text{mask}} \frac{t(y_m)}{r_1 r_2} e^{i\frac{2\pi}{\lambda}(r_1+r_2)} \\ &\times \left(\frac{\cos\theta_1 + \cos\theta_2}{2} \right) dy_m, \end{aligned}$$

where λ is the wavelength, and y_d and y_m are the vertical coordinates at the detector and mask, respectively. Also, r_1 and θ_1 are the distance and angle from the source point to the mask point at y_m, and r_2 and θ_2 are the distance and angle from the mask point y_m to the detector point y_d. $A_{\sigma,\pi}(\text{source})$ is the (angle-dependent) amplitude of the wave at the source point. Finally, $t(y_m)$ is the complex transmission function at the mask point y_m; this can be written as $t(y_m) = T(y_m)e^{i\delta(y_m)}$, where T is the real transmission and δ is the phase shift due to passage through the mask material at y_m. For materials which are common to all integration paths (mask substrate, diamond window, detector layers), the phase shifts are taken to be equal, and only the effects of the real attenuations are calculated.

For each pixel in the detector, the wavefront amplitude from each source point is calculated by the above integral, and converted to detected flux. The weighted flux contributions from source points are then summed over the source distribution. This process is repeated over the detectable spectral range, and the resulting simulated image is compared to measured image data.

PRELIMINARY MEASUREMENTS

A limited set of preliminary diagnostic measurements were taken during the January 2009 run. Fig. 2 shows the first image taken with white beam through the coded aperture mask. (In this case, the mask itself was scanned, as opposed to the detector pixel. Horizontal axis is mask offset projected onto detector plane.) As can be seen, the
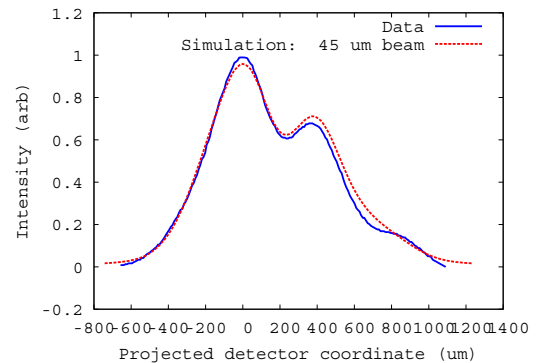

Figure 2: First scan: Image data for white beam, and simulated data for $45 \mu m$ beam.

best fit beam size, based on modulation depth between the two main peaks, is $\approx 45 \mu m$. This also agrees with other measurements made at the time using slits and Fresnel zone

plate, which all gave beam sizes in the range of $40-50\,\mu m$. However, the shape of the measured curve differs in some details from that of the simulated curve, most notably in the enhanced presence of the tertiary bump on the right hand shoulder.

A second scan was taken with a monochromator in place. The energy of the monochromator is estimated to have been ≈ 2.43 keV, though there was no opportunity to perform a calibration. The results of that scan (again, a mask scan rather than detector scan) are shown in Fig. 3. The best fit beam size based on simulation of a 2.43 keV monochromatic beam is $20\,\mu m$. For reference, Fresnel zone plate measurements taken around the same time (though not necessarily with the exact same beam conditions) indicated a beam size of $\approx 16-17\,\mu m$. Note again the enhanced prominence of the tertiary bump on the right hand shoulder in the measured data as compared to the somewhat smaller tertiary bump seen in the simulated curve.
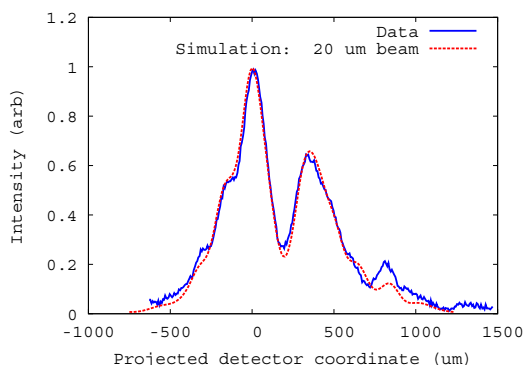

Figure 3: Image data for monochromatic beam, and simulated data for $20\,\mu m$ beam.
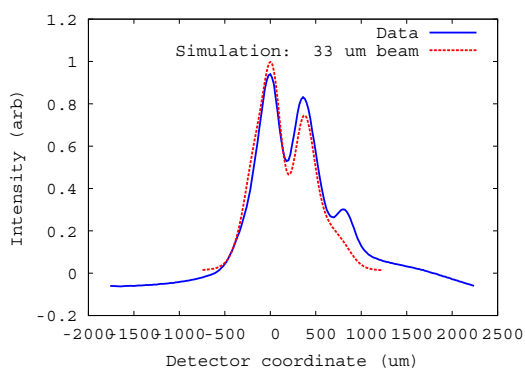

Figure 4: Data and simulation, white beam detector scan.

Finally, a detector scan with white beam is shown in Fig. 4. In this case the beam size appears to be around $33\,\mu m$, though the fit is not very good, with a range of fits of several μm. A monochromatic scan taken at 2.98 keV (not shown) agreed with the white beam scan, but again the measured curve shows some disagreement from the simulations in the ratios of the two main peaks, and in the prominence of

the tertiary peak. There were also some position-dependent variations in the background which suggest the possibility of a light leak affecting the measurements.

One possible reason for the enhanced prominence of the tertiary bump in the data is a limitation in the simulation. For now, the simulation is only 1-dimensional, in the vertical plane. For the next step a full 3-dimensional (in source distribution) and 2-dimensional (in mask and detector planes) simulation will be tried to see if the details such as the small bump on the right shoulder can be more accurately reproduced. With this we can also test for the possibility of rotational error between the mask and detector orientations. There may also be some unknown mask defects; new masks that are being made now and will be tested this summer should provide a useful comparison in that regard.

SUMMARY AND PROSPECTS

Preliminary measurements have been taken with a coded aperture mask at CesrTA in low-emittance mode. For beam profile reconstruction, a simulation method based on wavefront propagation is being developed taking into the full angular spectral distribution of the source flux and the wavelength-dependent transmissions and indices of refraction of all materials in the optical path and in the detector. Preliminary results indicate basic agreement with other methods of measuring the beam size using just a 1-D (vertical axis) simulation for source and mask. Future plans for improving the reconstruction of the detected image include full 3-D source and 2-D mask simulations. In addition, much more detailed data will be taken under various beam conditions in the coming months at CesrTA.

ACKNOWLEDGMENTS

REFERENCES

[1] J.W. Flanagan *et al.*, Proc. EPAC08, Genoa, 1029 (2008).

[2] R.H. Dicke, Astrophys. Journ., **153**, L101, (1968).

[3] E.E. Fenimore and T.M. Cannon, Appl. Optics, V17, No. 3, p. 337 (1978).

[4] J.P. Alexander *et al.*, TH5RFP026, elsewhere in these proceedings.

[5] W. Hopkins *et al.*, TH5RFP027, elsewhere in these proceedings.

[6] K.J. Kim, AIP Conf. Proc 184 (1989).

[7] S.G. Lipson, H. Lipson and D.S. Tannhauser, "Optical Physics," (Third Edition), Cambridge University Press (1995).

[8] J.D. Jackson, "Classical Electrodynamics," (Second Edition), John Wiley & Sons, New York (1975),